Journal Pre-proof

Improving strength-ductility synergy of nano/ultrafine-structured Al/Brass composite by cross accumulative roll bonding process

Majid Naseri, Mohsen Reihanian, Ahmad Ostovari Moghaddam, Davood Gholami, Seyedmehdi Hosseini, Mohammad Alvand, Ehsan Borhani, Evgeny Trofimov

PII: S2238-7854(23)02173-7

DOI: https://doi.org/10.1016/j.jmrt.2023.09.046

Reference: JMRTEC 8453

To appear in: *Journal of Materials Research and Technology*

Received Date: 1 August 2023

Revised Date: 3 September 2023

Accepted Date: 6 September 2023

Please cite this article as: Naseri M, Reihanian M, Moghaddam AO, Gholami D, Hosseini S, Alvand M, Borhani E, Trofimov E, Improving strength-ductility synergy of nano/ultrafine-structured Al/Brass composite by cross accumulative roll bonding process, *Journal of Materials Research and Technology*, https://doi.org/10.1016/j.jmrt.2023.09.046.

Improving strength-ductility synergy of nano/ultrafine-structured Al/Brass composite by cross accumulative roll bonding process

Majid Naseri [1,2,*], Mohsen Reihanian[3], Ahmad Ostovari Moghaddam[1,4], Davood Gholami[5], Seyedmehdi Hosseini[6,7], Mohammad Alvand[7], Ehsan Borhani[2], Evgeny Trofimov[1]

1) South Ural State University, 76 Lenin Av., Chelyabinsk 454080, Russia.
2) Department of Nanotechnology, Faculty of New Sciences and Technologies, Semnan University, Semnan, Iran.
3) Department of Materials Science and Engineering, Faculty of Engineering, Shahid Chamran University of Ahvaz, Ahvaz, Iran.
4) Advanced Materials and Nanotechnology Research Lab, Department of Materials Science and Engineering, K. N. Toosi University of Technology, Tehran, Iran.
5) School of Metallurgy and Materials Engineering, Iran University of Science and Technology, Tehran, Iran.
6) Brunel Centre for Advanced Solidification Technology (BCAST), Brunel University London, Uxbridge, UB8 3PH, UK.
7) Faculty of Materials and Metallurgical Engineering, Semnan University, Semnan, Iran.
*Corresponding Author. E-mail address: majid_na3ri@yahoo.com & naserim@susu.ru (M. Naseri)

Abstract

Increasing the strength of metallic multilayered composites fabricated through accumulative roll bonding (ARB) is typically accompanied by a sacrifice in ductility. In the current work, we propose a strategy to achieve microstructural refinement and outstanding strength-ductility synergy in Al/Brass composites. Here, the aluminum matrix exhibits a bimodal grain distribution, consisting of fine equiaxed grains with an average size of ~100 nm and ultrafine-elongated grains, in which the brass fragments were distributed uniformly. These microstructural features, introduced through cross accumulative roll bonding (CARB), provide synergistic strengthening effects. The CARB processed composite exhibits a mean misorientation angle of 43.16° and a fraction of high angle grain boundaries of 87%, compared to values of 38.02° and 79% for ARB processed specimen. The CARB processed composite demonstrates a major texture characterized by prominent Rotated Brass {110}<556>, Rotated Goss {011}<011>, and Rotated Cube {001}<110> components. In contrast, the ARB processed specimen revealed strong Goss {011}<100>, Rotated Goss {011}<011>, Brass {011}<211>, and S {123}<634> components. The Copper {112}<111> and S {123}<634> components were nearly absent in the CARB processed composite, because both of them were unstable under the CARB regime. The CARB processed composite shows a tensile strength of 405 MPa and a remarkable elongation of 12.4% at ambient temperature, outperforming ARB processed specimen with a tensile strength of 335 MPa and elongation of 9.5%. These unique mechanical properties in the CARB processed composite are ascribed to the dislocation strengthening, bimodal grain size distribution, uniformity of the brass fragments, and quality of bonding at the interfaces.

Keywords: Metallic multilayered composites; Severe plastic deformation; Microstructure characterization; Deformation texture; Mechanical properties.

1. Introduction

Light metal alloys have gained popularity due to the growing demand for lightweight structural materials with excellent strength-to-weight ratios, particularly in applications where weight plays a crucial role in the final product. The aerospace, automobile, and automotive industries have seen a continuous rise in the utilization of light metal alloys [1, 2]. Titanium and aluminum alloys as well as their composites are the main light metal alloys that have already undergone adaptation to innovative fabrication techniques. The average grain size is a fundamental microstructural feature that significantly influences the mechanical characterization of crystalline materials. Severe plastic deformation (SPD) is an effective process for inducing high strain in materials, thereby achieving high strength in both fine-grained and ultrafine-grained (UFG) materials [3-5]. Equal-channel angular pressing (ECAP), high-pressure torsion (HPT), accumulative roll bonding (ARB), and cross accumulative roll bonding (CARB) are currently the most popular SPD processes.

ARB, first invented by Japanese scientists in 1998 [6], can produce UFG metallic materials in the form of sheets with excellent mechanical properties. The conventional ARB is based on repeatedly rolling of two or more folded sheets with a typically 50% reduction in thickness, which causes individual layers to become permanently bonded via diffusion phenomena and friction forces between the components [6, 7]. The atomic bonding that takes place on a micro-scale and the mechanical bonding that occurs on a macro-scale both lead to the interfacial bonding. Methods based on ARB have the potential to be applied in the industry and are among the well-known plastic processing techniques with high strain. In contrast to other SPD methods, ARB has the additional advantage of being applicable to the continuous manufacturing of large-sized homogenous and metal matrix composites (MMCs). Over the past decade, the development of microstructures and their corresponding mechanical properties [8-20], wear and weldability

characteristics [21-27], and corrosion behavior of the ARB processed specimens [28-31] have been investigated for several alloys and aluminum based metal matrix composites.

Metallic multilayered composites have generated considerable interest owing to their potential usage in cutting-edge applications. Recently, these composites, which are incompatible with conventional bonding techniques, have also been produced using the ARB [32-36]. In dissimilar multi-layered systems, plastic flow instabilities manifest earlier in one layer due to differences in mechanical characteristics. Reihanian and Naseri have for the first time predicted how much strain is required to cause necking and fracture in metallic multilayer composites during ARB [37]. Based on the model, the critical strain for necking increases as the thickness ratio increases, the strength coefficient ratio increases, and the work-hardening exponent increases. However, the critical strain decreases as the soft phase work-hardening exponent increases. In the fabrication of metallic multilayered composites, ARB technique is naturally used to further improve the mechanical properties of the composites by increasing the layers and refining the grains [38, 39].

The microstructure of metals primarily affects their mechanical properties, meanwhile, processing routes greatly determine the microstructure of metals. In terms of rolling sheets and strips, there are two main processes: traditional single-directional rolling and cross-rolling processes. The effect of the cross-rolling process on the microstructure and properties of different metals has been already studied [40-42]. These studies demonstrated that the microstructure and mechanical properties are significantly influenced through the rolling processes (rolling direction). Additionally, numerous studies have shown that cross-rolling can significantly enhance the isotropic characteristics and texture distribution of metal sheets [43, 44]. Therefore, when the structure characteristics of metallic multilayered composites are the same, the mechanical properties are mostly determined by their microstructure and processing routes. ARB and CARB

are the two main rolling routes for fabricating metallic multilayered composites. Reports on CARB have mostly focused on single metals or composites [8, 9, 45-47]. Therefore, there is high anticipation to fabricate the metallic multilayered composites using the CARB.

It is important to investigate the effects of CARB on the mechanical properties of multilayered composites in order to enhance the isotropy of properties and maintain uniformity in microstructure and texture. As the name suggests, the focus of this study is on CARB processed Al/Brass composites. In order to determine whether CARB has a more significant effect on microstructure and mechanical properties, the specimens were compared with ARB processed specimens. Results from this research can be used to optimize the roll bonding technology for dissimilar metals and adjust the anisotropy of metallic multilayered composites fabricated by accumulative roll bonding process.

2. Experimental procedures

Commercially pure aluminum alloy sheet of thickness 1 mm and brass alloy sheet of thickness 0.8 mm were used as raw materials (specifications are given in Table 1). Parallel to the sheet rolling direction (RD), the sheets were cut into strips of 150 mm (length) × 50 mm (width). The next step in the materials processing procedure was annealing, conducted for aluminum and brass at 370°C and 500°C respectively, for 2 h to eliminate the effects of the previous step's induced deformation.

Table 1. Chemical composition (wt.%) of the aluminum and brass strips used in this study.

Al 1050									
Al	Si	Fe	Cu	Mn	Mg	Zn	Cr	Ni	Ti
97.3	0.588	0.762	0.189	0.732	0.189	0.129	0.0123	0.0058	0.0329
Be	Ca	Li	Pb	Sn	Sr	V	Na	Bi	Zr
< 0.0001	< 0.0009	< 0.0001	0.0049	0.0021	< 0.0001	0.0117	0.0043	< 0.005	< 0.002

B	Ga	Cd	Co	Ag	Hg	In			
0.005	0.0041	< 0.001	< 0.003	< 0.001	< 0.003	< 0.01			
Brass									
Cu	Zn	Pb	Sn	P	Mn	Fe	Ni	Si	Mg
61.3	38.4	< 0.005	< 0.005	< 0.003	0.0043	0.0269	0.0055	0.0183	0.0052
Cr	Al	S	As	Ag	Co	Bi	Cd	Sb	Zr
0.0024	0.0042	0.0074	0.0024	0.006	0.0088	0.0191	0.0009	0.0081	0.0036

The schematic illustration of the CARB for fabricating Al/Brass composite is shown in Fig. 1. The sheets were layered after surface preparation, with two aluminum layers on the outer surfaces and one brass layer on the inside surfaces. They were then fastened by copper wires at both ends in preparation for roll-bonding. After roll-bonding with 64% reduction in thickness (equivalent to 1.18 strain) in a single cycle, the sandwich sheets were cut in half (first round). In the second round of roll bonding, the sandwich sheets were stacked on top of each other, then degreased and brushed. A 90° rotation was then performed on the sheets around the ND axis. The roll-bonding process was carried out with a draft reduction of 50% (equivalent to 0.8 strain per cycle) on the rotating strip. During this stage, the strip was roll-bonded in the transverse direction (TD) of the previous stage. At ambient temperature, the same procedure was repeated up to eight cycles. For comparison, a specimen was subjected to ARB using the same parameters as CARB, but without rotation between successive cycles.

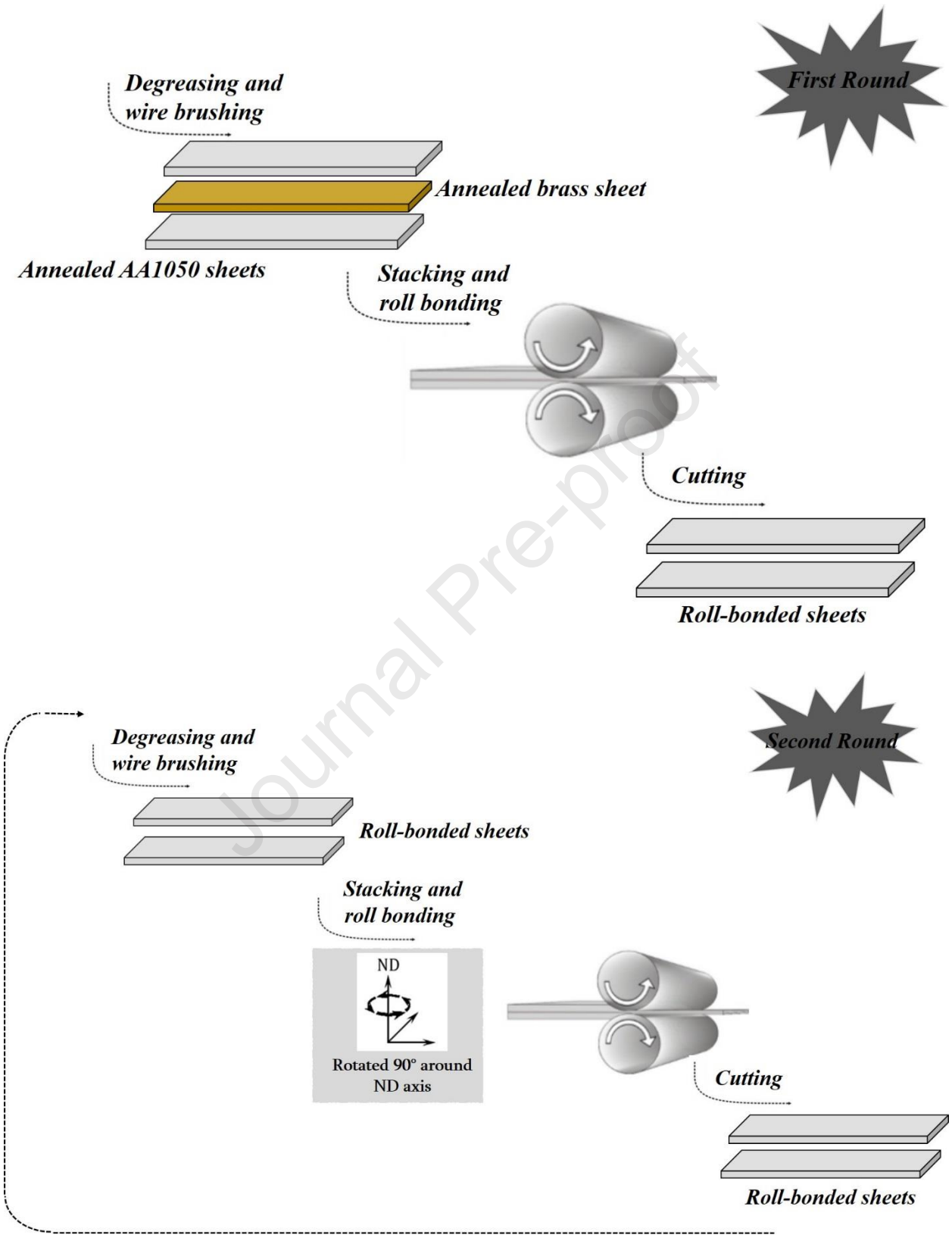

Fig. 1. *Schematic illustration showing the principle of CARB for fabricating Al/Brass composite.*

The microstructure evolution of the specimens were investigated by scanning transmission electron microscopy (STEM, JEOL JEM-2100F) and electron backscatter diffraction (EBSD) in a field emission scanning electron microscope (FESEM, Philips XL30). Microstructural investigation was done on the rolling direction-normal direction (RD-ND) and rolling direction-transverse direction (RD-TD) planes. In preparation for STEM characterization, a Thermo Fisher Scientific Helios G4 apparatus equipped with a focus ion beam (FIB) was used. To reduce noise in the STEM images presented herein, inverse fast Fourier transforming (IFFT) was performed with Gatan Digital Micrograph™ software. The morphology of the specimens was determined using transmission Kikuchi diffraction (TKD) with settings of 15 kV and 6.4 nA in the FIB system. The sheets' normal direction (ND) was selected as the reference axis for all inverse pole figure (IPF) maps. The electron backscatter diffraction (EBSD) measurements were performed using a step size of 50 nm. The acquired EBSD data, which were used to investigate the grain morphology and crystallographic texture, were analyzed by TSL-OIMTM (EDAX, USA) software.

Tensile tests were conducted on the specimens after different cycles using ISO 6892–01 standard. The tensile samples' gauge width and length were 5 ± 1 mm and 10 ±1 mm, respectively. The tensile tests were performed using a Hounsfield H50KS tensile testing equipment (Tinius Olsen Ltd, Redhill, UK) with an initial strain rate of 10^{-3} s^{-1}. To ensure the accuracy, each sample was tested three times. Additionally, the fracture surfaces of the tensile specimens were also inspected using a field emission scanning electron microscope (FESEM, VEGA\\TESCAN).

3. Results and discussion

3.1. Microstructural observation

Al/Brass composites' microstructure variation on the rolling direction-normal direction (RD-ND) plane following various ARB and CARB cycles are shown in Fig. 2. In the first cycle of composite production (Fig. 2(a)), it is clear that the brass layers are coherent and there is no crack or cavity at the interface of the layers. However, as the ARB cycles increase, the localized necking and fracture initiation can be observed (Figs. 2(b-d)). In general, necking and fracture predominately occur in the hard phase during the simultaneous deformation of dissimilar metals with differing flow properties. Plastic instability is influenced by variables like the initial thickness ratio, strength coefficients, and work-hardening exponents of the layers [37]. In the case of the Al/Brass system, brass serves as the hard phase and undergoes necking initially. Other studies additionally demonstrated the occurrence of necking in the hard phase in various multilayer systems [38, 48, 49].

With an increase in the number of ARB cycles, the applied strain is intensified, leading to a reduction in the thickness of brass layers. Consequently, the brass layer experience rupture in the fourth cycle. After eight ARB cycles, the resulting aluminum matrix composite exhibits a nearly homogeneous distribution of brass fragments, which act as the reinforcement phase (Fig. 2(e)). Fig. 2(b′) indicates that necking and rupturing in the brass layers substantially occur after the second CARB cycle. This can be attributed to the fact that the CARB process involves roll-bonding the specimens parallel and perpendicular to the RD in successive cycles by rotating the strip around the ND. Repeated necking and fracturing of the brass layers due to an increase in CARB cycles eventually leads to the formation of brass fragments (see Figs. 2(c′-e′)). Fig. 2 represents the SEM/elemental mapping of Al, Cu, and Zn elements after eight cycles of both ARB and CARB processes. The SEM/elemental maps confirm the occurrence of necking, rupturing and

fragmentation in the brass layers. Moreover, it is evident from the maps that the brass fragments are distributed more uniformly within the aluminum matrix during CARB compared to ARB.

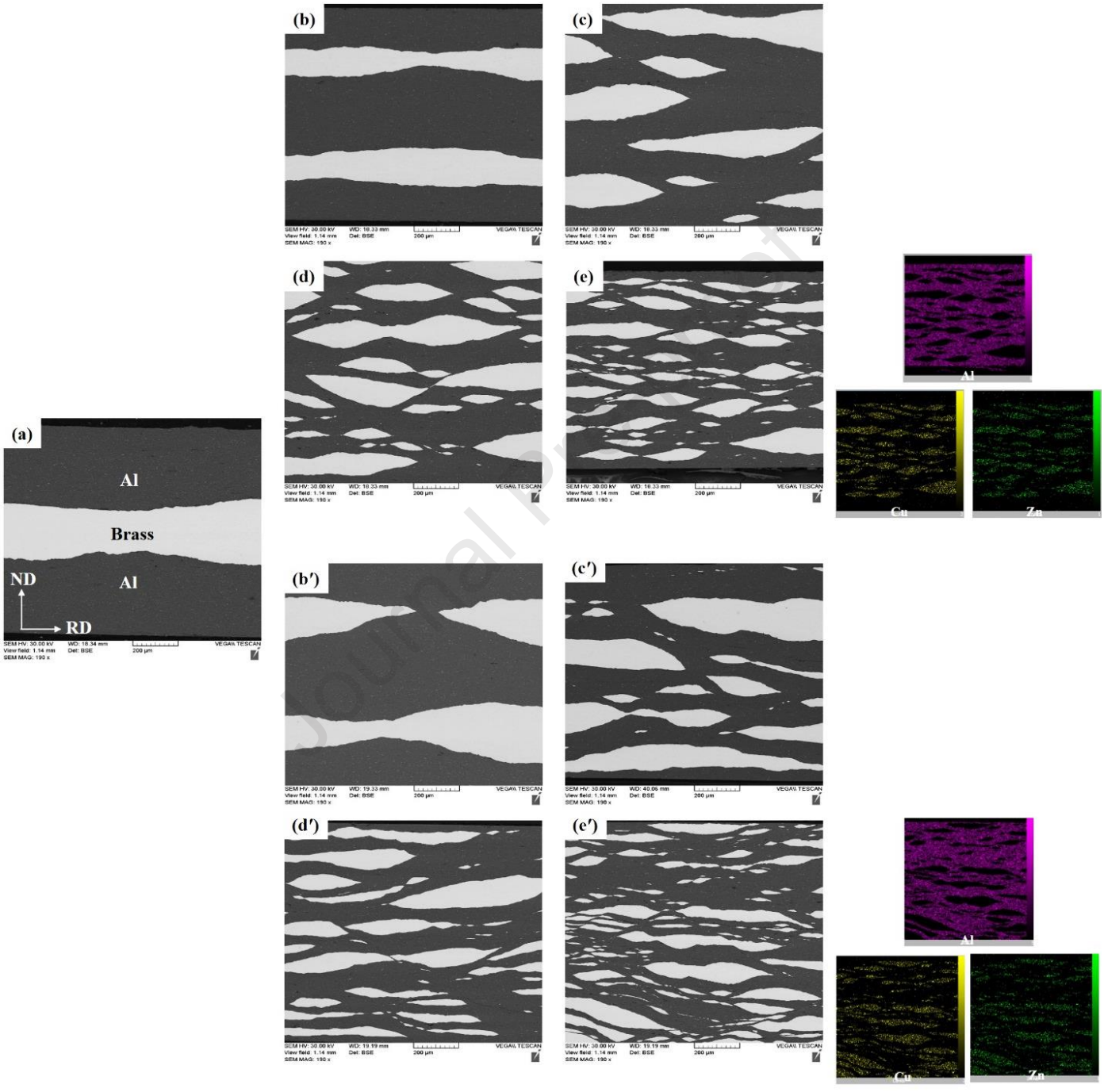

Fig. 2. *SEM micrographs of ARB ((a)-(e)) and CARB ((b')-(e')) processed Al/Brass composite after (a) one, (b) and (b') two, (c) and (c') four, (d) and (d') six, and (e) and (e') eight cycles, along with the corresponding EDS maps.*

The thickness of the brass layers is variable in different regions, as clearly shown in Figs. 2(e and e′). Brass layers are thinner around the rolling surface than they are in the center. This is explained by the shear strain brought about by the friction between the specimen and the rolling mills. It is also notable that distinct waviness is present, which is caused by shear bands that are formed during the ARB and CARB processes. According to previous research [50, 51], localized deformation may lead to the formation of shear bands at an angle of 45° to the rolling direction. Shear bands pass through the aluminum layers because more active slip systems are available in the softer layers (aluminum). Brass layers, on the other hand, are less deformable and show discontinuity when shear bands reach the interface between aluminum and brass layers. As well as contributing to necking and fractures, shear bands also promote fragmentation and decrease the thickness of brass layers.

STEM and selected area diffraction (SAD) patterns from the RD-TD plane of the Al/Brass composites after the eighth cycle are depicted in Fig. 3. In the case of the ARB processed Al/Brass composite (Fig. 3(a-c)), the SAD pattern is characterized by a ring pattern consisting of discrete spots, indicating the presence of a substantial number of grains (polycrystalline material). The average grain size is ~200-250 nm, and the distribution of grain size is relatively uniform throughout the RD-TD plane. On the other hand, for the CARB processed Al/Brass composite (Fig. 3(d-e)), a more uniform distribution of fine grains is observed. There are numerous dislocation tangles at grain boundaries and within sub-grains. There is dispersion of lamellar microstructure along the TD direction due to the change in rolling direction between CARB cycles. As the number of CARB cycles increases, the microstructure becomes more uniform, and the lamellar microstructure exhibits no distinct preferred orientation.

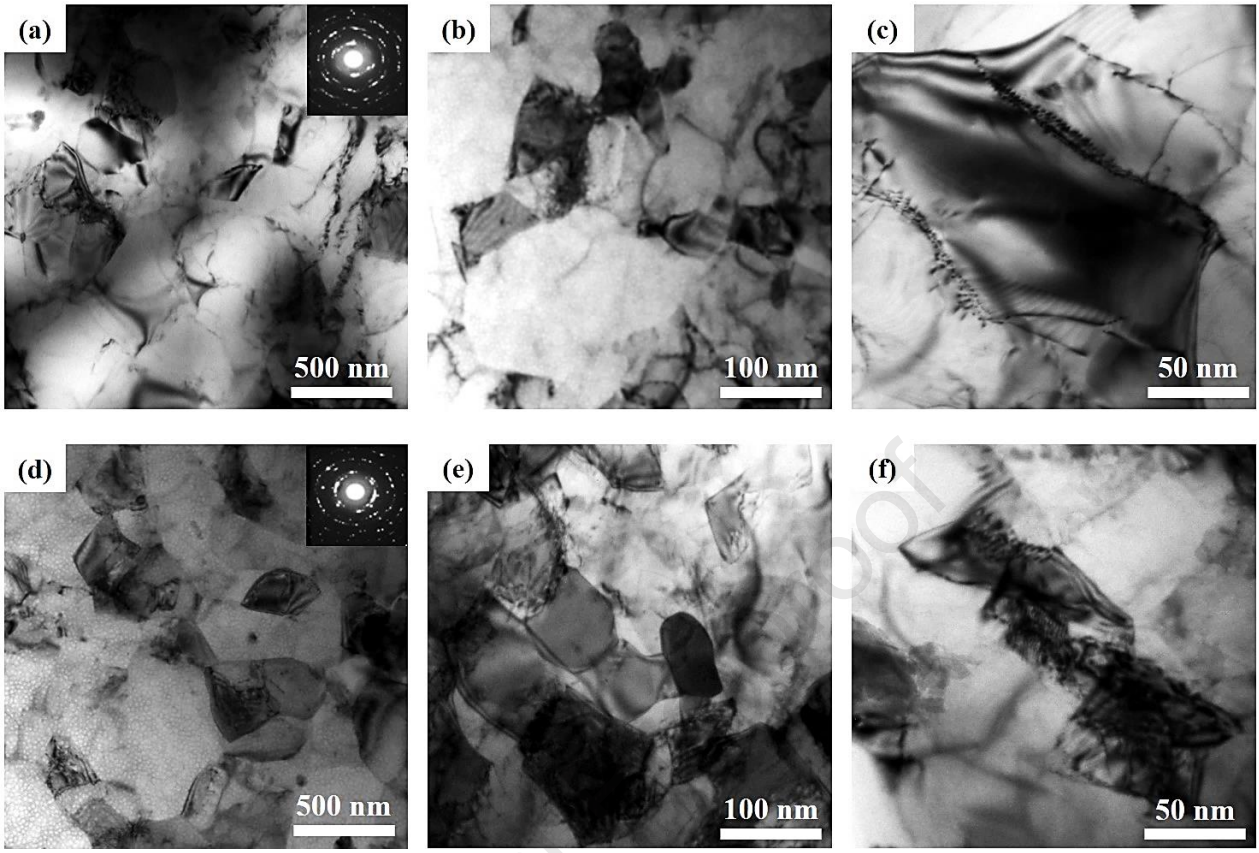

Fig. 3. *STEM micrographs and the matching SAD patterns from the RD–TD plane of Al/Brass composite after eight (a-c) ARB and (d-f) CARB cycles taken at different magnifications.*

In the CARB processed Al/Brass composite, the diffraction spots in the SAD pattern appear as a ring, indicating a more pronounced orientation difference between the grains. Additionally, the average grain size of the CARB processed Al/Brass composite is approximately 100-150 nm, which is smaller than that of ARB processed composite. Furthermore, there is a slightly higher presence of dislocations in the CARB processed composite. Also, isolated spots in the SAD pattern of the CARB processed Al/Brass composite indicate a decrease in orientation difference. A rotating dynamic recrystallizing mechanism is triggered as CARB accumulates strain, resulting in fine grains forming in the macroscopic shear bands [52-54]. As compared with the ARB specimen, the CARB composite has a much more homogeneous microstructure after eight cycles, consisting

of fine recrystallized grain. CARB specimens also have a significantly higher density of dislocation forests than ARB specimens.

The EBSD inverse pole figure (IPF) map, orientation color map, and misorientation angle distribution of the Al/Brass composites after eight cycles are illustrated in Fig. 4. On the boundary maps, red lines indicate low angle grain boundaries (LAGBs) with misorientation angles between 2–15° degrees, while green lines indicate high angle grain boundaries (HAGBs) with misorientation angles more than 15°. Furthermore, the EBSD data were used to calculate the mean misorientation angle of the boundaries (θ_m) and the fraction of high angle grain boundaries (f_{HAGB}). As shown clearly in Fig. 4(a), ARB results in bimodal microstructure consisting of fine recrystallized and elongated aluminum grains along the RD with a relatively large aspect ratio after eight cycles. In the ARB processed Al/Brass composite, the mean boundary spacing along the RD (length of the elongated grains) and the average lamellar boundary spacing along the ND (thickness of the elongated grains) are ~750 ± 10 nm and ~280 ± 10 nm, respectively. Additionally, the average size of equiaxed grains after eight ARB cycles is about ~250 nm, showing significant grain refining. Additionally, nanometric grains (less than 100 nm) can be observed. ARB-processed materials, particularly single-phase alloys, have also been observed to produce ultrafine grains.

After eight CARB cycles (Fig. 4(b)), the microstructure is characterized primarily by equiaxed grains and some elongated grains with a lower aspect ratio than the ARB specimen. There is clearly an increase in ultrafine-grained regions compared to the ARB specimen. As a result of a change in the processing route, grains will be nearly equiaxed. It can be seen that after eight cycles, θ_m and f_{HAGB} for the ARB processed Al/Brass composite are 38.02° and 79%, respectively, whereas for the CARB processed Al/Brass composite, these parameters are 43.16° and 87%. The CARB

processed Al/Brass composite also has a more uniform microstructure, with an average grain size of 100 nm. The obtained results suggest that a nanostructured Al/Brass composite can be achieved via CARB.

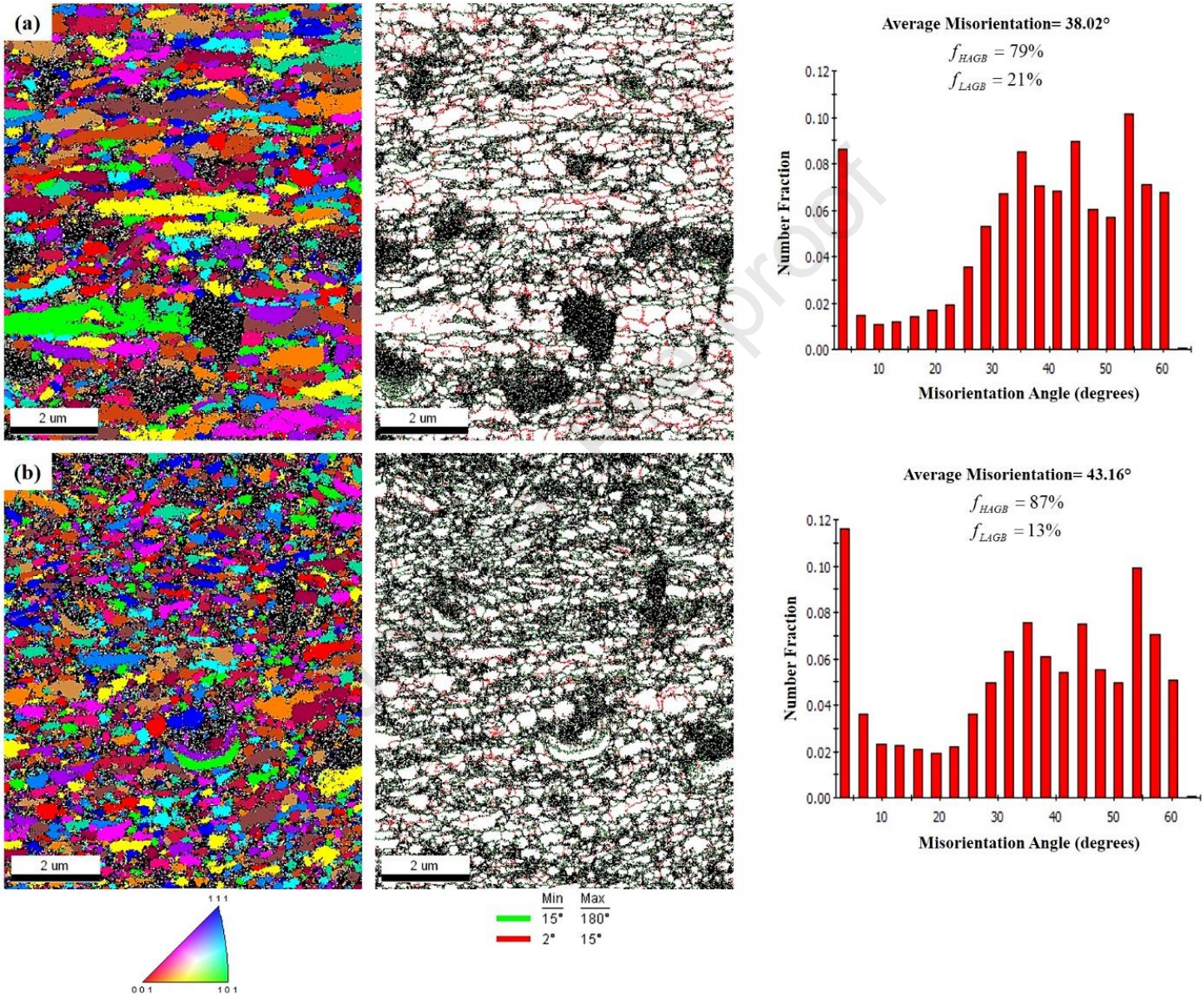

Fig. 4. *EBSD inverse pole figure (IPF) map, orientation color map, and misorientation angle distribution from RD–ND plane of the (a) ARB and (b) CARB processed Al/Brass composite after eight cycles.*

Generally, ARB processed materials exhibit two different types of grain boundaries: (i) extended lamellar boundaries (LBs) and (ii) short transverse boundaries (TBs). Transverse boundaries exhibit a characteristic bamboo-like structure and are typically observed in lamellar boundaries. The rolling direction and lamellar boundaries are roughly parallel (grain elongation direction) [51, 55, 56]. As can be seen in Fig. 4 compared to the ARB processed specimen, the CARB processed specimen shows fewer lamellar boundaries (LBs) and interconnecting boundaries. Therefore, the CARB processed specimen has a less elongated structure and a smaller grain size than the ARB processed specimen. In the CARB process, lamellar boundaries alternate from being parallel to RD to being perpendicular in the next cycle. It is important to note, however, that the lamellar boundaries in the ARB remain parallel to RD throughout all cycles. In addition, after each CARB cycle, the specimen rotates about the ND axis, resulting in an increase in stored energy and, in turn, the driving force for continuous and discontinuous recrystallization [57].

The orientation distribution functions (ODFs) of the annealed aluminum, ARB, and CARB Al/Brass composites after eight cycles are shown in Fig. 5. The φ_2 = 0°, 45°, and 65° sections are displayed since they contain all necessary face-centered cubic (FCC) deformation texture components. Textural components of the annealed aluminum can be characterized as Brass {011}<211>, S {123}<634>, and Cube {001}<100> components with a maximum intensity of 6.9 × R, 6.2 × R, and 5.4 × R, respectively (Fig. 5(a)). After eight ARB cycles (Fig. 5(b)), the Goss {011}<100> and Rotated Goss {011}<011> components with a maximum intensity of 13.1 × R and 11.3 × R, respectively, are created, and the intensity of the Brass {011}<211> and S {123}<634> components increased to 12.5 × R and 7.4 × R, respectively. The development of the Rotated Brass {110}<556>, Rotated Goss {011}<011>, and Rotated Cube {001}<110> components is clearly evident in CARB processed Al/Brass composite (Fig. 5(c)). The maximum

intensities of the Rotated Brass {110}<556>, Rotated Goss {011}<011>, and Rotated Cube {001}<110> components are 21.5 × R, 11.5 × R, and 7.4 × R, respectively, in the CARB processed specimen.

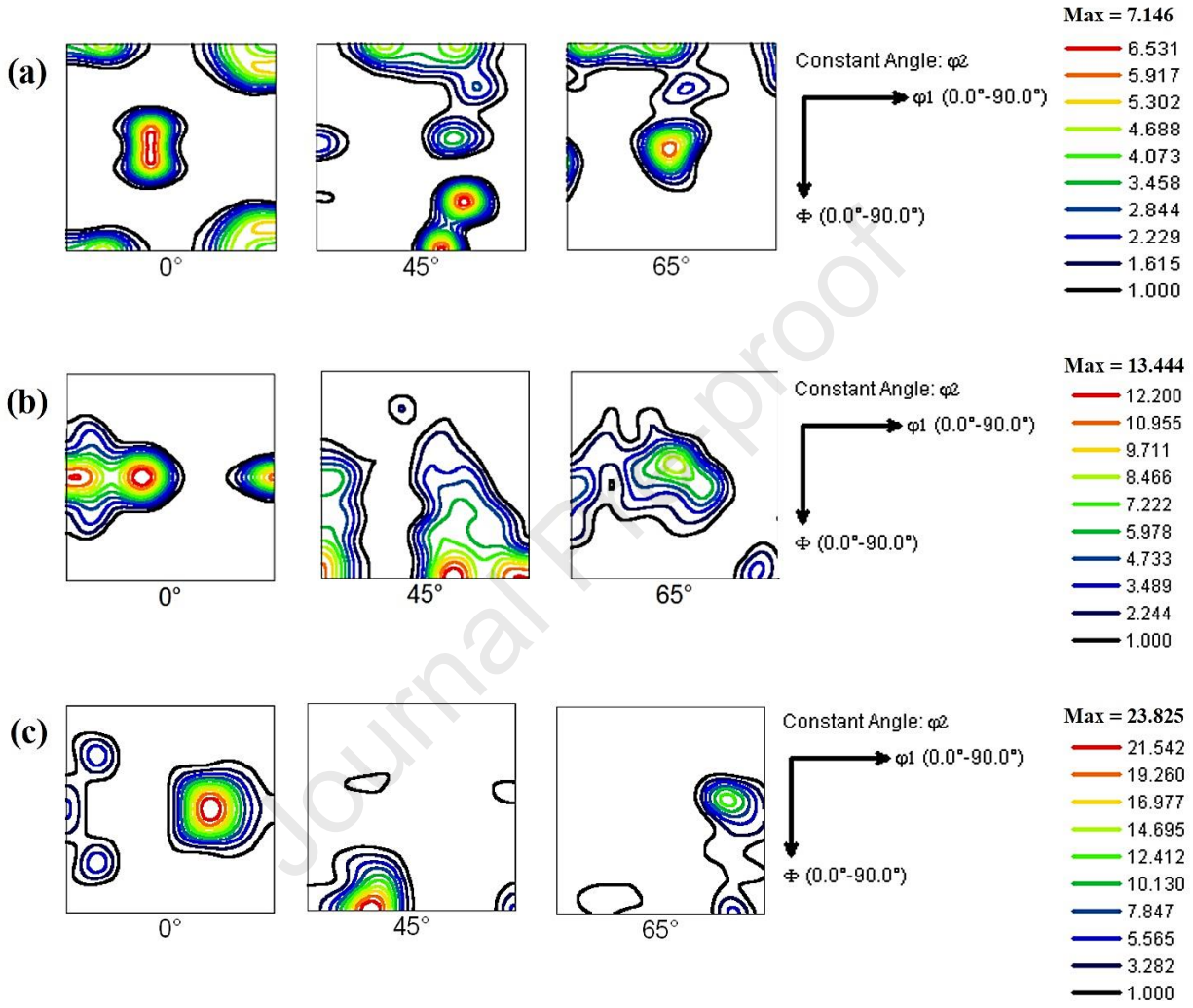

Fig. 5. *The ODF sections at constant angles (0º, 45º, and 65º) showing the texture components in the (a) annealed aluminum, (b) ARB, and (c) CARB processed Al/Brass composite after eight cycles.*

For the ARB processed Al/Brass composite, a mixed deformation/recrystallization texture can be depicted from the ODFs in Fig. 5. It is well known that the texture forms around the Copper {112}<111>, Brass {011}<211> and S {123}<634> orientations during plane strain deformation

of aluminum alloys (as in the case of rolling) and in the absence of recrystallization [58]. In metals with low or medium stacking fault energies (SFE), such as copper, brass, and austenitic iron, where recovery processes are delayed, recrystallization may take occur when a threshold degree of deformation is created. Also, recrystallization occurs at a lower temperature and in a shorter period of time as the amount of strain increases [57]. In consequence, recrystallization intensifies with increased ARB cycles. The recrystallization of the Al/Brass composite also helps to generate equiaxed grains (see Fig. 4(a)) rather than elongated grains at higher ARB cycles. It is sensible to attribute recrystallization to the presence of Goss {011}<100> and Rotated Goss {011}<011> orientations in the CARB processed Al/Brass composite. From the ODF sections, it can be verified that the Copper {112}<111> and S {123}<634> components are nearly absent in the CARB processed Al/Brass composite due to their instability under the CARB regime where the rolling direction is changed after each cycle.

3.2. Mechanical properties

Fig. 6 shows how the tensile strength of Al/Brass composites varies with the number of rolling cycles. Likewise, the engineering stress-strain curves of the annealed aluminum, ARB, and CARB processed Al/Brass composites after eight cycles are presented in Fig. 7. It is evident that the tensile strength of the specimens improves with an increasing number of rolling cycles. After the first cycle, the tensile strength of the specimens increased by 153%, from 78 MPa (for the annealed aluminum) to 197 MPa. Previous study [32, 33, 35, 38, 49] has shown that the first cycle has a considerable influence on tensile strength. ARB and CARB gradually increase tensile strength to 335 MPa and 405 MPa, respectively, about 4.3 and 5.2 times the strength of annealed aluminum. This indicates that the Al/Brass composite is effectively strengthened during ARB and CARB due

to two factors: (i) grain refinement and (ii) homogeneous distribution of brass layers, which act as reinforcement in the aluminum matrix.

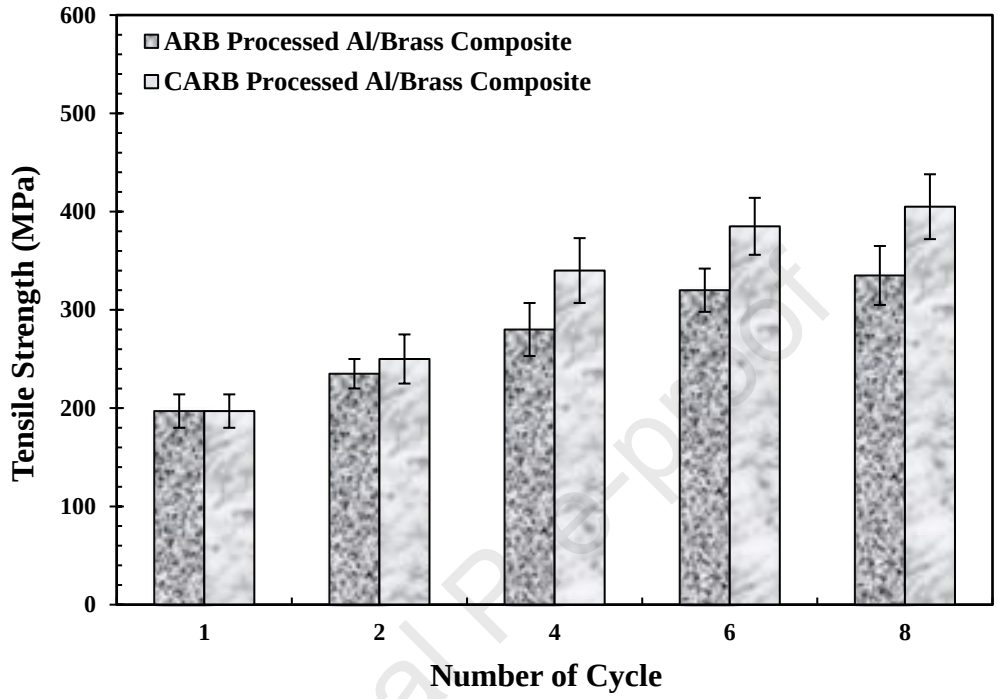

Fig. 6. *Variations in the tensile strength with the number of rolling cycles for ARB and CARB processed Al/Brass composites.*

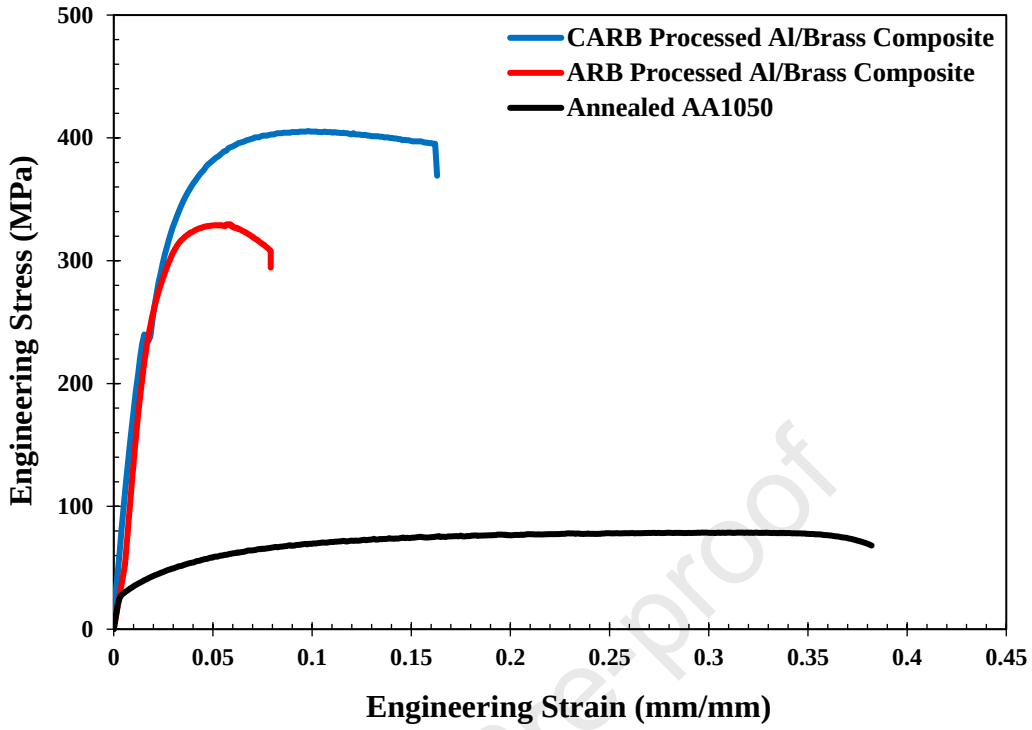

Fig. 7. *Stress-strain curves for annealed aluminum, eight-cycle ARB and CARB processed Al/Brass composites.*

The mechanisms of strain hardening and grain refinement play crucial roles in the variations of tensile strength observed in SPD processed specimens. In the initial stages of the ARB and CARB, strain hardening is the dominant factor, boosting the strength of the specimens, accompanied by the formation of submicron subgrains or dislocation cells. Nevertheless, as the number of rolling cycles increase, grain refinement becomes the dominant mechanism, exerting control over the strengthening process. Consequently, the gradual evolution of ultrafine grains contributes to the significant increase in specimen strength [59].

The CARB processed Al/Brass composite has a higher tensile strength than the ARB processed Al/Brass composite in all cycles. By rotating the strip around the ND axis, new slip is activated after each CARB cycle. A latent hardening effect is produced by dislocation interactions between primary slip systems and active or non-active slip systems. It should be pointed out that the strength

of metallic multilayered composites is influenced by the size, shape, and distribution of the reinforcement phase. The strength of the composite increases as the reinforcement phase becomes smaller and its distribution becomes more uniform. After eight CARB cycles, the brass layers change from an elongated shape to small and thin fragments (see Fig. 2), exhibiting a more homogeneous distribution than the ARB specimen. Additionally, it is well known that specimens processed with CARB have higher strengths owing to the better bonding quality between the layers [8, 9].

The variation in the elongation of the ARB and CARB processed Al/Brass composites with the number of rolling cycles is presented in Fig. 8. In the case of the annealed specimen, the elongation dropped from 36% to 8.8% after the first cycle, a 75% decrease. The strain hardening, reduction of dislocations mobility especially in brass layers, and the development of weak longitudinal interfaces between the aluminum layers are responsible for the substantial decrease in the elongation after the first rolling cycle. With increasing rolling cycles, however, the elongation improves, especially with the CARB process. The elongation increased from 8.8% (after the first cycle) to 9.5% and 12.4% after eight cycles, indicating improvements of 10% and 30% for the ARB and CARB processed Al/Brass composites, respectively.

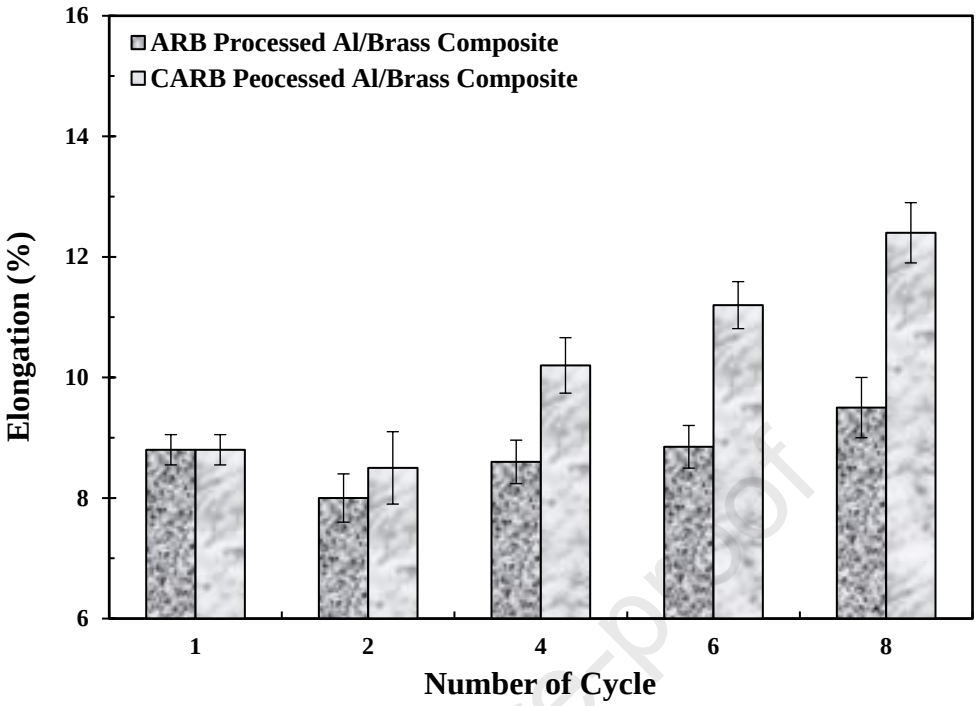

Fig. 8. *Variations in elongation with the number of rolling cycles for ARB and CARB processed Al/Brass composites.*

It has been reported that strain hardening, interface bonding, and the distribution of constituent phases are the main factors affecting the elongation of metallic multilayered composites during ARB [34, 35, 60, 61]. The strain hardening-induced increase in dislocation density and buildup of internal stresses enhance the initiation of fractures and reduce elongation. On the other hand, bonding and continuity at interfaces, can boost elongation by delaying crack formation at the interface. Furthermore, when the distribution of constituent phases in the matrix becomes more uniform, the elongation increases because the net distance between the interfaces increases.

It has been claimed that one of the weaknesses of SPD processed materials is a lack of ductility [62, 63]. In Al/Brass composites, elongation decreases in the first cycle due to the reduction of dislocation mobility. By proceeding the ARB, the elongation increases because of the strengthening of the bonding between the layers and the improved distribution of constituent

phases in the matrix. CARB processed Al/Brass composites show a higher elongation than ARB specimens for all rolling cycles. This is mainly due to grain refinement and a better distribution of brass fragments in the aluminum matrix. According to the microstructural observations, CARB processed Al/Brass composites have smaller grains and refined brass fragments with smaller aspect ratios that are distributed more uniformly in the aluminum matrix compared to the ARB specimens (see Figs. 2 and 4).

3.3. Fractography

After the tensile test, the fracture surfaces of the annealed aluminum, ARB, and CARB treated Al/Brass composites are illustrated in Fig. 9. The fracture surface of all the specimens is characterized by the formation of dimples and a fibrous appearance, which are characteristics of ductile fracture [64]. During ductile fracture, microvoids form and coalesce, resulting in crack growth with slow tear, excessive plastic deformation, and rough fracture surfaces with equiaxed and deep dimples. The deep and equiaxed dimples in the annealed aluminum specimen are seen in Fig. 9(a and b). According to our previous studies [12, 26, 30], the size and shape of the dimples change as the number of rolling cycles increases. As seen in Fig. 9 ((c and d) and (e and f)), there is some difficulty in identifying the individual layers due to an increase in layer number and a decrease in layer thickness. Equiaxed dimples in Al/Brass composites processed by ARB and CARB become shallower, smaller, and more elongated. The formation of dimples has also been observed on the fracture surface of Al/Mg [61], Al/Cu [65], Al/Al-Zn-Mg-Cu [66], and Ni/Ti/Al/Cu [33] systems. On the fracture surfaces of the ARB processed Al/Brass composite, smaller and elongated dimples are present, indicating a lower degree of ductility than the CARB specimen.

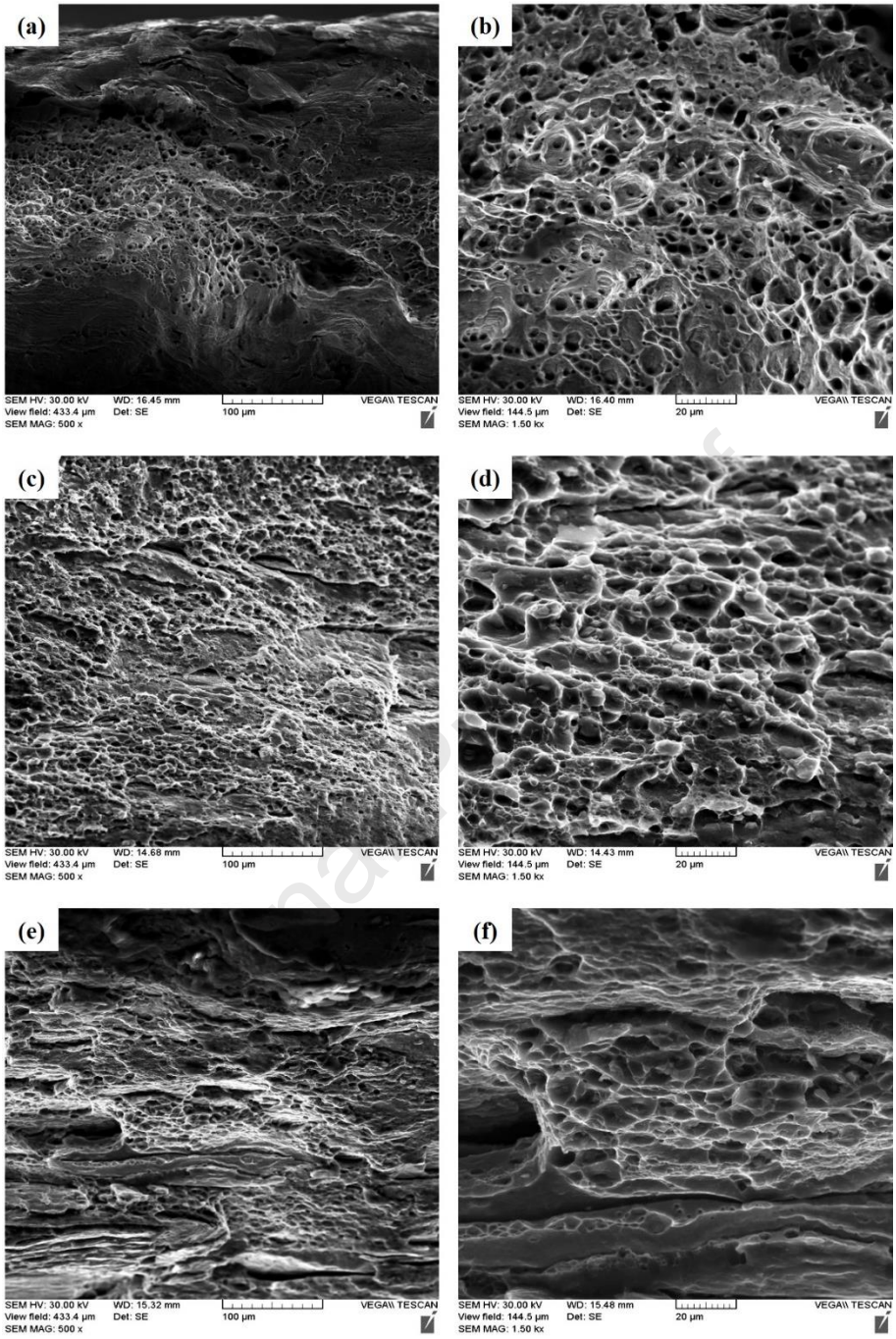

Fig. 9. *SEM micrographs of the fracture surfaces after the tensile test for: (a and b) annealed aluminum, (c and d) ARB, and (e and f) CARB processed Al/Brass composites.*

In summary, the CARB processed Al/Brass composite offers a significant advantages with the formation of a bimodal structure comprising equiaxed grains, ultrafine-elongated grains, and brass

fragments. Synergistic strengthening effects are provided by this unique structure, which surpasses the bamboo-like structure of the ARB specimen. As a result, it enhances the potential for dislocations stalling, multiplication and accumulation, leading to a strain hardening rate that yields unexpected elongation for SPD processed materials. Further studies are required to comprehensively understand the underlying mechanisms of the ARB routes responsible for developing a bimodal microstructure and promoting the strength–ductility synergy in nanostructured metals.

4. Conclusions

In the current study, nano/ultrafine-structured Al/Brass composite is successfully fabricated using two different processing routes: accumulative roll bonding (ARB) and cross accumulative roll bonding (CARB). Microstructure characterization and mechanical properties with strength-ductility synergy are systematically studied. Our results can be summarized as follows:

1. Necking and fracture of the brass hard layer occur during the CARB, resulting in a metallic multilayered composite with a more uniform distribution of brass fragments after eight CARB cycles compared to ARB.
2. The microstructure of the CARB specimen is characterized by equiaxed grains and some elongated grains with a lower aspect ratio than in the ARB specimen. Moreover, the CARB specimen exhibits an increased fraction of ultrafine-grained regions. During successive cycles of strip rotation around the normal direction (ND), lamellar boundaries alternately become parallel and perpendicular to the rolling direction (RD).
3. After eight CARB cycles, the texture components in the CARB processed Al/Brass composite are Rotated Brass {110}<556>, Rotated Goss {011}<011>, and Rotated Cube

{001}<110> components. Meanwhile, the ARB processed specimen revealed Goss {011}<100>, Rotated Goss {011}<011>, Brass {011}<211>, and S {123}<634> components.

4. High tensile strength (~405 MPa) and good elongation (~12.4%) are simultaneously obtained for the CARB processed Al/Brass composite. The high strength is derived from the presence of hard nano/ultrafine grains, the back stress induced by the matrix/reinforcement interfaces, and the uniform distribution of the brass fragments.
5. In contrast to ARB, achieving a reasonable ductility in the CARB processed Al/Brass composite can be ascribed to the multiplication of plentiful forest dislocations, which are induced by the bimodal grain structure and various matrix/reinforcement interfaces.
6. All specimens exhibit dimples on their fracture surfaces, which are a typical ductile fracture mechanism. On the fracture surfaces of the CARB processed Al/Brass composite, large and semi-equiaxed dimples are observed, indicating a higher degree of ductility compared to the ARB specimen.

CRediT authorship contribution statement

Majid Naseri: Conceptualization, Investigation, Validation, Writing – Original Draft, Writing – Review & Editing. **Mohsen Reihanian:** Conceptualization, Validation, Writing – Review & Editing. **Ahmad Ostovari Moghaddam:** Writing – Review & Editing. **Davood Gholami:** Conceptualization, Investigation, Validation. **Seyedmehdi Hosseini**: Conceptualization, Validation, Writing – Review & Editing. **Mohammad Alvand:** Investigation, Validation. **Ehsan Borhani:** Conceptualization, Investigation, Validation, Project Administration. **Evgeny Trofimov:** Conceptualization, Validation, Writing – Review & Editing.

Acknowledgment

M. Naseri gratefully acknowledge the help of the research board of Shahid Chamran University of Ahvaz, Ahvaz, Iran for the provision of research facilities for this project during the Doctor of Philosophy (Ph.D) course. He is also grateful to Seoul National University, Seoul, South Korea, for providing funding for this research under the Brain Korea 21 (BK21) Postdoctoral Fellowship. He is also most appreciative of Prof. H.W. Jang and Prof. M.R. Shokouhimehr for informative discussion and technical assistance in FIB-TEM and EBSD experiments. This work was also financially supported by Ministry of Science and Higher Education of the Russian Federation (FENU-2023-0013).

References

[1] E. Schubert, M. Klassen, I. Zerner, C. Walz, G. Sepold, Light-weight structures produced by laser beam joining for future applications in automobile and aerospace industry, Journal of Materials Processing Technology 115(1) (2001) 2-8.

[2] S.Z. Han, E.A. Choi, S.H. Lim, S. Kim, J. Lee, Alloy design strategies to increase strength and its trade-offs together, Progress in Materials Science 117 (2021) 100720.

[3] R.Z. Valiev, 1 - Producing bulk nanostructured metals and alloys by severe plastic deformation (SPD), in: S.H. Whang (Ed.), Nanostructured Metals and Alloys, Woodhead Publishing 2011, 3-39.

[4] R.Z. Valiev, R.K. Islamgaliev, I.V. Alexandrov, Bulk nanostructured materials from severe plastic deformation, Progress in Materials Science 45(2) (2000) 103-189.

[5] Y. Estrin, A. Vinogradov, Extreme grain refinement by severe plastic deformation: A wealth of challenging science, Acta Materialia 61(3) (2013) 782-817.

[6] Y. Saito, N. Tsuji, H. Utsunomiya, T. Sakai, R.G. Hong, Ultra-fine grained bulk aluminum produced by accumulative roll-bonding (ARB) process, Scripta Materialia 39(9) (1998) 1221-1227.

[7] N. Tsuji, Y. Saito, H. Utsunomiya, S. Tanigawa, Ultra-fine grained bulk steel produced by accumulative roll-bonding (ARB) process, Scripta Materialia 40(7) (1999) 795-800.

[8] M. Naseri, A. Hassani, M. Tajally, An alternative method for manufacturing Al/B_4C/SiC hybrid composite strips by cross accumulative roll bonding (CARB) process, Ceramics International 41(10) (2015) 13461-13469.

[9] M. Naseri, M. Reihanian, E. Borhani, Effect of strain path on microstructure, deformation texture and mechanical properties of nano/ultrafine grained AA1050 processed by accumulative roll bonding (ARB), Materials Science and Engineering: A 673 (2016) 288-298.

[10] M. Naseri, A. Hassani, M. Tajally, Fabrication and characterization of hybrid composite strips with homogeneously dispersed ceramic particles by severe plastic deformation, Ceramics International 41(3) (2015) 3952-3960.

[11] M. Naseri, M. Reihanian, E. Borhani, A new strategy to simultaneous increase in the strength and ductility of AA2024 alloy via accumulative roll bonding (ARB), Materials Science and Engineering: A 656 (2016) 12-20.

[12] M. Reihanian, F.K. Hadadian, M.H. Paydar, Fabrication of Al–2 vol% Al_2O_3/SiC hybrid composite via accumulative roll bonding (ARB): An investigation of the microstructure and mechanical properties, Materials Science and Engineering: A 607 (2014) 188-196.

[13] E. Bagherpour, M. Reihanian, H. Miyamoto, Tailoring particle distribution non-uniformity and grain refinement in nanostructured metal matrix composites fabricated by severe plastic deformation (SPD): a correlation with flow stress, Journal of Materials Science 52(6) (2017) 3436-3446.

[14] M. Askarpour, Z. Sadeghian, M. Reihanian, Role of powder preparation route on microstructure and mechanical properties of Al-TiB_2 composites fabricated by accumulative roll bonding (ARB), Materials Science and Engineering: A 677 (2016) 400-410.

[15] S.H. Lee, Y. Saito, N. Tsuji, H. Utsunomiya, T. Sakai, Role of shear strain in ultragrain refinement by accumulative roll-bonding (ARB) process, Scripta Materialia 46(4) (2002) 281-285.

[16] N. Tsuji, Y. Ito, Y. Saito, Y. Minamino, Strength and ductility of ultrafine grained aluminum and iron produced by ARB and annealing, Scripta Materialia 47(12) (2002) 893-899.

[17] W.S. Barakat, M. Kh. Younis, A.M. Sadoun, A. Fathy, M.I.A. Habba, Optimization of the accumulative roll bonding process parameters and SiC content for optimum enhancement in mechanical properties of Al-Ni-SiC composites, Alexandria Engineering Journal 76 (2023) 131-151.

[18] M. I. A. Habba, M. Kh. Younis, A.M. Sadoun, A. Fathy, W.S. Barakat, On the microstructural and mechanical responses of dual-matrix Al-Ni/SiC composites manufactured using accumulative roll bonding, Alexandria Engineering Journal 78 (2023) 1-14.

[19] I.M.R. Najjar, A.M. Sadoun, M.A. Elaziz, H. Ahmadian, A. Fathy, A.M. Kabeel, Prediction of the tensile properties of ultrafine grained Al–SiC nanocomposites using machine learning, Journal of Materials Research and Technology 24 (2023) 7666-7682.

[20] G.S. Alsoruji, A.M. Sadoun, M.A. Elaziz, M.A. Al-Betar, A.W. Abdallah, A. Fathy, On the prediction of the mechanical properties of ultrafine grain Al-TiO_2 nanocomposites using a modified long-short term memory model with beluga whale optimizer, Journal of Materials Research and Technology 23 (2023) 4075-4088.

[21] R. Jamaati, M. Naseri, M.R. Toroghinejad, Wear behavior of nanostructured Al/Al_2O_3 composite fabricated via accumulative roll bonding (ARB) process, Materials & Design 59 (2014) 540-549.

[22] Y.S. Sato, Y. Kurihara, S.H.C. Park, H. Kokawa, N. Tsuji, Friction stir welding of ultrafine grained Al alloy 1100 produced by accumulative roll-bonding, Scripta Materialia 50(1) (2004) 57-60.

[23] Y.S. Sato, M. Urata, Y. Kurihara, S.H.C. Park, H. Kokawa, K. Ikeda, N. Tsuji, Microstructural Evolution during Friction Stir Welding of Ultrafine Grained Al Alloys, Materials Science Forum 503-504 (2006) 169-174.

[24] M. Naseri, M. Alvand, D. Gholami, E. Borhani, H. Abdollah-Pour, S. Fakhravar, Friction stir welding of nano/ultrafine-grained AA2024 alloy produced through an accumulative roll bonding process, MRS Communications 12(1) (2022) 51-57.

[25] I. Najjar, A. Sadoun, M.N. Alam, A. Fathy, Prediction of wear rates of Al-TiO_2 nanocomposites using artificial neural network modified with particle swarm optimization algorithm, Materials Today Communications 35 (2023) 105743.

[26] I.M.R. Najjar, A.M. Sadoun, A. Ibrahim, H. Ahmadian, A. Fathy, A modified artificial neural network to predict the tribological properties of Al-SiC nanocomposites fabricated by accumulative roll bonding process, Journal of Composite Materials 57(21) (2023) 3433-3445.

[27] I. Najjar, A. Sadoun, A. Fathy, On the understanding and prediction of tribological properties of Al-TiO2 nanocomposites using artificial neural network, Journal of Composite Materials 57(14) (2023) 2325-2337.

[28] M. Naseri, E. Borhani, O. Imantalab, H.W. Jang, M. Shokouhimehr, A. Fattah-alhosseini, Correlation between crystallographic texture and electrochemical behavior of nano/ultrafine-grained AA2024 alloy processed by accumulative roll bonding process, Journal of Materials Research and Technology 18 (2022) 4256-4266.

[29] A. Fattah-alhosseini, S.O. Gashti, Corrosion Behavior of Ultra-fine Grained 1050 Aluminum Alloy Fabricated by ARB Process in a Buffer Borate Solution, Journal of Materials Engineering and Performance 24(9) (2015) 3386-3393.

[30] A. Fattah-alhosseini, O. Imantalab, Effect of accumulative roll bonding process on the electrochemical behavior of pure copper, Journal of Alloys and Compounds 632 (2015) 48-52.

[31] A. Fattah-alhosseini, M. Naseri, M.H. Alemi, Corrosion behavior assessment of finely dispersed and highly uniform Al/B_4C/SiC hybrid composite fabricated via accumulative roll bonding process, Journal of Manufacturing Processes 22 (2016) 120-126.

[32] A. Mozaffari, H. Danesh Manesh, K. Janghorban, Evaluation of mechanical properties and structure of multilayered Al/Ni composites produced by accumulative roll bonding (ARB) process, Journal of Alloys and Compounds 489(1) (2010) 103-109.

[33] N. Ye, X. Ren, J. Liang, Microstructure and mechanical properties of Ni/Ti/Al/Cu composite produced by accumulative roll bonding (ARB) at room temperature, Journal of Materials Research and Technology 9(3) (2020) 5524-5532.

[34] G. Anne, M.R. Ramesh, H.S. Nayaka, S.B. Arya, Investigation of microstructure and mechanical properties of Mg–Zn/Al multilayered composite developed by accumulative roll bonding, Perspectives in Science 8 (2016) 104-106.

[35] H. Dong, Y. Chen, Y. Guo, G. Shan, G. Yang, L. Huang, F. Liu, Q. Li, A nanostructured Ag/Cu multilayered composite exhibiting high hardness and high electrical conductivity prepared by a novel multicomponent accumulative roll bonding, Materials Characterization 196 (2023) 112613.

[36] M. Naseri, M. Reihanian, E. Borhani, EBSD characterization of nano/ultrafine structured Al/Brass composite produced by severe plastic deformation, Journal of Ultrafine Grained and Nanostructured Materials 51(2) (2018) 123-138.

[37] M. Reihanian, M. Naseri, An analytical approach for necking and fracture of hard layer during accumulative roll bonding (ARB) of metallic multilayer, Materials & Design 89 (2016) 1213-1222.

[38] L. Ghalandari, M.M. Mahdavian, M. Reihanian, M. Mahmoudiniya, Production of Al/Sn multilayer composite by accumulative roll bonding (ARB): A study of microstructure and mechanical properties, Materials Science and Engineering: A 661 (2016) 179-186.

[39] K. Wu, H. Chang, E. Maawad, W.M. Gan, H.G. Brokmeier, M.Y. Zheng, Microstructure and mechanical properties of the Mg/Al laminated composite fabricated by accumulative roll bonding (ARB), Materials Science and Engineering: A 527(13) (2010) 3073-3078.

[40] P.P. Bhattacharjee, M. Joshi, V.P. Chaudhary, M. Zaid, The effect of starting grain size on the evolution of microstructure and texture in nickel during processing by cross-rolling, Materials Characterization 76 (2013) 21-27.

[41] H. Chen, Y. Han, C. Liu, Z. Chen, Effect of unidirectional rolling and cross-rolling on microstructure and mechanical anisotropy of Mg-Gd-Y-Ag-Zr plates, Journal of Alloys and Compounds 960 (2023) 170680.

[42] P. Zhang, Y. Xin, L. Zhang, S. Pan, Q. Liu, On the texture memory effect of a cross-rolled Mg-2Zn-2Gd plate after unidirectional rolling, Journal of Materials Science & Technology 41 (2020) 98-104.

[43] W. Liu, X. Li, X. Meng, Effect of pseudo cross-rolling on the recrystallization texture of a continuous cast Al–Mg alloy, Scripta Materialia 60(9) (2009) 768-771.

[44] N. Nayan, S. Mishra, A. Prakash, S.V.S.N. Murty, M.J.N.V. Prasad, I. Samajdar, Effect of cross-rolling on microstructure and texture evolution and tensile behavior of aluminium-copper-lithium (AA2195) alloy, Materials Science and Engineering: A 740-741 (2019) 252-261.

[45] M. Alizadeh, A. Shakery, E. Salahinejad, Aluminum-matrix composites reinforced with E-glass fibers by cross accumulative roll bonding process, Journal of Alloys and Compounds 804 (2019) 450-456.

[46] M.R. Kamali Ardakani, S. Khorsand, S. Amirkhanlou, M. Javad Nayyeri, Application of compocasting and cross accumulative roll bonding processes for manufacturing high-strength, highly uniform and ultra-fine structured Al/SiC_p nanocomposite, Materials Science and Engineering: A 592 (2014) 121-127.

[47] M. Alizadeh, E. Salahinejad, Processing of ultrafine-grained aluminum by cross accumulative roll-bonding, Materials Science and Engineering: A 595 (2014) 131-134.

[48] L. Song, H. Gao, L. Bhatt, C. Kong, H. Yu, Microstructure and mechanical properties of AA1050/AA6061 multilayer composites via accumulative roll bonding and cryorolling and subsequent aging, Materials Science and Engineering: A 874 (2023) 145069.

[49] N.E. Mahallawy, A. Fathy, W. Abdelaziem, M. Hassan, Microstructure evolution and mechanical properties of Al/Al–12%Si multilayer processed by accumulative roll bonding (ARB), Materials Science and Engineering: A 647 (2015) 127-135.

[50] D.C. Camilo Magalhães, O.M. Cintho, J.B. Rubert, V.L. Sordi, A.M. Kliauga, The role of shear strain during accumulative roll-bonding of multilayered composite sheets: Pattern formation, microstructure and texture evolution, Materials Science and Engineering: A 796 (2020) 140055.

[51] N. Kamikawa, T. Sakai, N. Tsuji, Effect of redundant shear strain on microstructure and texture evolution during accumulative roll-bonding in ultralow carbon IF steel, Acta Materialia 55(17) (2007) 5873-5888.

[52] D. Kuhlmann-Wilsdorf, Theory of plastic deformation: - properties of low energy dislocation structures, Materials Science and Engineering: A 113 (1989) 1-41.

[53] R.Z. Valiev, B. Straumal, T.G. Langdon, Using severe plastic deformation to produce nanostructured materials with superior properties, Annual Review of Materials Research 52(1) (2022) 357-382.

[54] A. Keyvani, M. Naseri, O. Imantalab, D. Gholami, K. Babaei, A. Fattah-alhosseini, Microstructural characterization and electrochemical behavior of nano/ultrafine grained pure copper through constrained groove pressing (CGP), Journal of Materials Research and Technology 11 (2021) 1918-1931.

[55] N. Tsuji, 2 - Bulk nanostructured metals and alloys produced by accumulative roll-bonding, in: S.H. Whang (Ed.), Nanostructured Metals and Alloys, Woodhead Publishing 2011, pp. 40-58.

[56] B.L. Li, N. Tsuji, N. Kamikawa, Microstructure homogeneity in various metallic materials heavily deformed by accumulative roll-bonding, Materials Science and Engineering: A 423(1–2) (2006) 331-342.

[57] T. Sakai, A. Belyakov, R. Kaibyshev, H. Miura, J.J. Jonas, Dynamic and post-dynamic recrystallization under hot, cold and severe plastic deformation conditions, Progress in Materials Science 60 (2014) 130-207.

[58] V. Yousefi Mehr, M.R. Toroghinejad, On the texture evolution of aluminum-based composites manufactured by ARB process: A review, Journal of Materials Research and Technology 21 (2022) 1095-1109.

[59] I. Sabirov, M.Y. Murashkin, R.Z. Valiev, Nanostructured aluminium alloys produced by severe plastic deformation: New horizons in development, Materials Science and Engineering: A 560 (2013) 1-24.

[60] P. Qu, L. Zhou, V.L. Acoff, Deformation textures of aluminum in a multilayered Ti/Al/Nb composite severely deformed by accumulative roll bonding, Materials Characterization 107 (2015) 367-375.

[61] H.S. Liu, B. Zhang, G.P. Zhang, Microstructures and Mechanical Properties of Al/Mg Alloy Multilayered Composites Produced by Accumulative Roll Bonding, Journal of Materials Science & Technology 27(1) (2011) 15-21.

[62] Y. Wang, M. Chen, F. Zhou, E. Ma, High tensile ductility in a nanostructured metal, Nature 419(6910) (2002) 912-915.

[63] M.A. Meyers, A. Mishra, D.J. Benson, Mechanical properties of nanocrystalline materials, Progress in Materials Science 51(4) (2006) 427-556.

[64] T.H. Courtney, Mechanical Behavior of Materials, McGraw Hill Custom Pub.2000.

[65] V. Yousefi Mehr, M.R. Toroghinejad, A. Rezaeian, Mechanical properties and microstructure evolutions of multilayered Al–Cu composites produced by accumulative roll bonding process and subsequent annealing, Materials Science and Engineering: A 601 (2014) 40-47.

[66] S.H.S. Ebrahimi, K. Dehghani, J. Aghazadeh, M.B. Ghasemian, S. Zangeneh, Investigation on microstructure and mechanical properties of Al/Al-Zn-Mg–Cu laminated composite fabricated by accumulative roll bonding (ARB) process, Materials Science and Engineering: A 718 (2018) 311-320.

Declaration of interests

The authors declare that they have no known competing financial interests or personal relationships that could have appeared to influence the work reported in this paper.